Title

Why estimates of deglacial ice loss should be biased low

Authors

Gebbie, Geoffrey
Simms, Alexander R
Lisiecki, Lorraine E

Publication Date

2019-06-01

DOI

10.1016/j.epsl.2019.03.017

Peer reviewed

Earth and Planetary Science Letters 515 (2019) 112–124

Contents lists available at ScienceDirect

Earth and Planetary Science Letters

www.elsevier.com/locate/epsl

Why estimates of deglacial ice loss should be biased low

Geoffrey Gebbie [a,*], Alexander R. Simms [b], Lorraine E. Lisiecki [b]

[a] Department of Physical Oceanography, Woods Hole Oceanographic Institution, 360 Woods Hole Rd., MS # 29, Woods Hole, MA 02543, USA
[b] Department of Earth Science, University of California, Santa Barbara, CA, USA

ARTICLE INFO

Article history:
Received 15 May 2018
Received in revised form 27 February 2019
Accepted 12 March 2019
Available online 28 March 2019
Editor: R. Bendick

Keywords:
paleoceanography
physical oceanography
ice sheets
Last Glacial Maximum
inverse methods

ABSTRACT

Sea level rose by about 130 m over the last deglaciation, but the Last Glacial Maximum (LGM, 24,000 to 18,000 yr before present) is estimated to have had only enough grounded ice to raise sea level by about 115 m. These estimates of the mass of grounded ice are typically expressed as an equivalent sea-level rise by normalizing with the oceanic surface area and seawater density. Here we diagnose the deglacial freshwater budget by comparing the freshwater content of the modern ocean to four reconstructions of the Last Glacial Maximum constrained by data from porewaters, benthic foraminifera, and faunal assemblages. A deglacial ice loss of 127.4 to 128.0 m of sea-level equivalent is necessary to balance the freshwater budget, suggesting a bias of 2.0 to 2.6 m less than the assumed true sea-level rise. Oceanic thermal expansion explains 0.8 to 1.4 m of the bias. Independent of deglacial warming, an additional 1.2 m of bias is intrinsic to the formulation of the equivalent sea-level metric. Thus, estimates of deglacial ice loss should underestimate the true sea-level rise, leading to a reduction in the amount of glacial land ice that needs to be found.

1. Introduction

Far-field estimates of sea-level rise since the Last Glacial Maximum are converging upon a value of 132 ± 2 m (1σ) when corrected for isostatic adjustment (Austermann et al., 2013; Lambeck et al., 2014; Nakada et al., 2016). The amount of land ice that existed during the LGM, however, is estimated to sum to 114 ± 9 m of sea level equivalent (e.g., Simms et al., 2019). Thus, ice loss estimates appear to be 19 ± 10 m too small to explain the post-LGM sea-level rise. The discrepancy is large enough that a missing ice sheet has been hypothesized over the present-day East Siberian margin (e.g., Clark and Tarasov, 2014).

The difference between inferred ice loss and sea-level rise may be statistically insignificant due to the underestimation of errors in the problem. For example, the far-field sea-level reconstructions are largely based on data from just three locations: Barbados (Fairbanks, 1989; Peltier and Fairbanks, 2006; Austermann et al., 2013), the Bonaparte Gulf (e.g., Yokoyama et al., 2000), and the Sunda Shelf (e.g., Hanebuth et al., 2000). Multiple estimates of the size of individual LGM ice sheets are available, but they often do not agree within their published errors (see Table 1, Simms et al., 2019).

Physical processes may also explain why ice loss estimates do not add up to the full sea-level rise. The flow of groundwater into the ocean would raise sea level, but an analysis of modern-day aquifers indicates that the contribution could be no more than 1.4 m (Simms et al., 2019). Another potential explanation is the effect of seawater expansion. The ocean warmed over the deglaciation, where the resulting expansion yields a greater sea-level rise for a given mass of added meltwater. Here, the focus is on the changing seawater density, under acknowledgment that other statistical and physical processes, such as those discussed above, may also be important.

In this work, new information about deglacial changes in seawater density and freshwater content from recently-derived temperature and salinity reconstructions of the LGM (Gebbie, 2012, 2014; Gebbie et al., 2015; Bereiter et al., 2018) are compiled. In particular, we use the fully nonlinear thermodynamic equation of state (IOC, SCOR, and IAPSO, 2010) to compute seawater density change and the oceanic freshwater budget over the deglaciation. Proxy observations of LGM temperature and salinity are sparse, and therefore we document the sensitivity of our results by employing four LGM reconstructions derived from differing datasets. We find that the necessary ice loss, in terms of sea-level equivalent, is less than the true sea-level rise in a wide range of deglacial scenarios. A companion work (Simms et al., 2019) places these results into the wider context of observational uncertainties and groundwater discharge.

* Corresponding author.
E-mail address: ggebbie@whoi.edu (G. Gebbie).

https://doi.org/10.1016/j.epsl.2019.03.017
0012-821X/

2. Methods

2.1. Deglacial freshwater budget

The amount of freshwater added to the ocean should be identifiable, in concept, by the difference in the LGM and modern oceanic freshwater inventories. Changes in the oceanic mass of freshwater are here assumed to be entirely due to the addition of meltwater from grounded ice, as is approximately true if changes due to atmospheric water storage, groundwater storage, volcanic discharge, and sea-ice volume are relatively small. With these assumptions, the glacial-to-modern freshwater budget is,

$$M_m = M_g + \Delta M_{ice}, \tag{1}$$

where M_m and M_g are the masses of freshwater in the modern and glacial oceans, respectively, and the mass of ice, ΔM_{ice}, includes all ice loss on the continents (including ice grounded on continental shelves) (e.g., Lambeck et al., 2014). Thus, the mass of ice necessary to balance the budget is equal to the freshwater mass difference between the modern and LGM oceans, $\Delta M_{ice} = M_m - M_g$.

The mass of freshwater in the modern ocean is,

$$M_m = \int^{X}\int^{Y}\int_{Z_b}^{Z_m} (1 - S_m)\rho_m \, dz \, dy \, dx, \tag{2}$$

where X, Y, and Z are the longitudinal, latitudinal, and depth dimensions, respectively, Z_m is modern sea level, Z_b is the depth of the seafloor, S_m is the modern absolute salinity in units of mass of salt per mass of seawater, and ρ_m is the three-dimensional modern seawater density. The integrals are restricted to the volume of the ocean. Similarly, the freshwater mass of the LGM ocean is,

$$M_g = \int^{X}\int^{Y}\int_{Z_b}^{Z_g} (1 - S_g)\rho_g \, dz \, dy \, dx, \tag{3}$$

where S_g, ρ_g, and Z_g are the LGM values of salinity, seawater density, and sea level, respectively. For ease of notation, the freshwater content (i.e., the density of freshwater in seawater) is defined,

$$\tilde{\rho}_m = (1 - S_m)\rho_m, \;\; \tilde{\rho}_g = (1 - S_g)\rho_g, \tag{4}$$

where $(1 - S_m)$ and $(1 - S_g)$ are the freshwater mass fractions for the modern and LGM oceans and are bounded by 0 and 1 (e.g., Wijffels et al., 1992). The inferred mass of melted ice is equal to the difference in modern and glacial freshwater inventories,

$$\Delta M_{ice} = \int^{X}\int^{Y} \left\{ \int_{Z_b}^{Z_m} \tilde{\rho}_m \, dz - \int_{Z_b}^{Z_g} \tilde{\rho}_g \, dz \right\} dy \, dx, \tag{5}$$

where the limits of the integrals must vary depending on the oceanic area. The integrands on the right hand side are the freshwater mass of the modern and LGM oceans, respectively.

2.2. Equivalent sea-level rise from ice loss

The rate of sea-level rise depends upon both the mass of ice loss and the oceanic area over which the meltwater is spread (e.g., Lambeck and Chappell, 2001). In particular, the rate of change of oceanic volume is, $\partial V/\partial t = \partial[A\ \eta]/\partial t$, where V is oceanic volume, η is the sea level, and A is the horizontal area of the ocean that depends on the vertical coordinate. The LGM ocean had about 6% less area than the modern-day (Smith and Sandwell, 1997; Becker et al., 2009) and thus rates of sea-level rise would have been 6% greater for a given ice loss. Furthermore, the rate of change of volume depends upon the mass added to the ocean, as seen by expanding equation (62) of Griffies and Greatbatch (2012) to include the time-evolving oceanic area:

$$\frac{\partial[A\ \eta]}{\partial t} = \int^{X}\int^{Y} \frac{F_{ice}(x,y)}{\rho(x,y,\eta)} \, dy \, dx + n, \tag{6}$$

where the integral occurs over the oceanic area in the X and Y dimensions, $F_{ice}(x,y)$ is the meltwater input per area, $\rho(x,y,\eta)$ is the seawater density at the sea surface, and n is a term due to non-Boussinesq steric effects related to seawater density change (see Section 4, Griffies and Greatbatch, 2012). Thus, the relationship between meltwater input and sea-level rise is intricate.

Ice loss estimates are expressed as an equivalent sea-level rise by making three major assumptions: (1) meltwater input is spread evenly over the sea surface, (2) surface seawater density is well represented by a baseline value, ρ_0, and (3) non-Boussinesq steric effects are negligible. To convert glaciological estimates of ice loss to an equivalent sea-level rise, the relevant oceanic surface area must be applied, but this information is often not available in published estimates. For this reason, we introduce a fourth assumption, that the average deglacial oceanic area, A_{dg}, can be substituted for the time-varying area (see Appendix A for calculating A_{dg}). This assumption leads to an underestimate of sea-level rise in the first half of the deglaciation, but a compensating overestimate in the second half.

Under the foregoing assumptions, we now refer to the equivalent sea-level rise due to ice loss, $\Delta\eta_{ice}$, rather than the true sea-level rise, $\Delta\eta$. When applying these assumptions to equation (6), we obtain the rate of equivalent sea-level rise due to ice loss,

$$\frac{d\eta_{ice}}{dt} = \frac{1}{\rho_0\, A_{dg}} \frac{dM_{ice}}{dt}, \tag{7}$$

where ρ_0 is a reference seawater density, A_{dg} is the deglacial-average oceanic surface area, and dM_{ice}/dt is the global rate of meltwater input (i.e., $\int^X \int^Y F_{ice}\ dy\ dx$). Integrating (7) from the LGM to the modern-day (i.e., t_g to t_m), the equivalent sea-level rise over the deglaciation is defined as (e.g., Lambeck and Chappell, 2001),

$$\Delta\eta_{ice} = \frac{\Delta M_{ice}}{\rho_0\, A_{dg}}, \tag{8}$$

where the oceanographic quantities on the right hand side are related to the glaciological estimates of the size of different ice sheets on the left hand side (e.g., Clark and Tarasov, 2014).

An explicit form of $\Delta\eta_{ice}$ is formed by combining equations (5) and (8),

$$\Delta\eta_{ice} = \frac{1}{A_{dg}} \int^{X}\int^{Y} \left\{ \int_{Z_b}^{Z_m} \frac{\tilde{\rho}_m}{\rho_0} \, dz - \int_{Z_b}^{Z_g} \frac{\tilde{\rho}_g}{\rho_0} \, dz \right\} dy \, dx, \tag{9}$$

an ice-loss estimate inferred from the oceanic freshwater budget that is independent from glaciological estimates. Equation (9) is referred to as the "deglacial ice loss estimate" in the rest of this work.

2.3. Bias in deglacial ice loss estimates

Our focus is determining the potential bias in ice loss estimates when posed as an equivalent sea-level rise. To isolate the bias,

we assume that far-field estimates of a deglacial sea-level rise of $\Delta\eta = 130$ m are correct (e.g., Clark et al., 2009) and that sea-level rose uniformly. The assumption that sea-level rose uniformly rules out the possibility to detect changes in local sea level due to circulation change, but global-mean sea-level rise should be unaffected by the redistribution of mass by the circulation. Following the definition of A_{dg} in Appendix A and the rules for integral limits, the true sea-level rise, $\Delta\eta$, is expressed in a form that is useful for comparison to equation (9),

$$\Delta\eta = \frac{1}{A_{dg}} \int^{X} \int^{Y} \left\{ \int_{Z_b}^{Z_m} dz - \int_{Z_b}^{Z_g} dz \right\} dy\, dx. \tag{10}$$

The bias in deglacial ice loss is the difference between the true sea-level rise and ice-loss estimates, $B \equiv \Delta\eta - \Delta\eta_{ice}$, and is diagnosed by subtracting equation (9) from (10) to obtain,

$$B = \frac{1}{A_{dg}} \int^{X} \int^{Y} \left\{ \int_{Z_b}^{Z_m} \frac{\rho_0 - \tilde{\rho}_m}{\rho_0}\, dz - \int_{Z_b}^{Z_g} \frac{\rho_0 - \tilde{\rho}_g}{\rho_0}\, dz \right\} dy\, dx. \tag{11}$$

The quantity inside the curly brackets,

$$\Delta h = \int_{Z_b}^{Z_m} \frac{\rho_0 - \tilde{\rho}_m}{\rho_0}\, dz - \int_{Z_b}^{Z_g} \frac{\rho_0 - \tilde{\rho}_g}{\rho_0}\, dz, \tag{12}$$

represents the deglacial change in the height of a freshwater column relative to that of seawater with density, ρ_0. The bias in ice-loss estimates is the area-weighted average of the height change from each water column,

$$B = \frac{1}{A_{dg}} \int^{X} \int^{Y} \Delta h\, dy\, dx, \tag{13}$$

which permits the regional sources of the bias to be diagnosed through the horizontally-varying field, Δh.

To understand the unintuitive quantity, Δh, it is decomposed with the definition of freshwater content to yield,

$$\Delta h = \int_{Z_b}^{Z_m} \left(\frac{\rho_0 - \rho_m}{\rho_0} + \frac{S_m \rho_m}{\rho_0} \right) dz - \int_{Z_b}^{Z_g} \left(\frac{\rho_0 - \rho_g}{\rho_0} + \frac{S_g \rho_g}{\rho_0} \right) dz. \tag{14}$$

We define Δh_ρ and Δh_s to be the LGM-to-modern height change due to seawater density and mass of salt, respectively,

$$\Delta h_\rho = \int_{Z_b}^{Z_m} \frac{\rho_0 - \rho_m}{\rho_0} dz - \int_{Z_b}^{Z_g} \frac{\rho_0 - \rho_g}{\rho_0} dz,$$

$$\Delta h_s = \int_{Z_b}^{Z_m} \frac{S_m \rho_m}{\rho_0}\, dz - \int_{Z_b}^{Z_g} \frac{S_g \rho_g}{\rho_0}\, dz, \tag{15}$$

where these two factors explain the total change, i.e., $\Delta h = \Delta h_\rho + \Delta h_s$. Note that salt affects both terms, through the mass of the salt and by the effect of salinity on density.

If seawater expands, then Δh_ρ is positive and less ice loss is needed for a given sea-level rise. The quantity, Δh_ρ, appears to be related to the steric height (e.g., Gill and Niiler, 1973), but here is calculated with a fixed ρ_0 in the denominator rather than a changing reference density with pressure. Later we show that Δh_ρ is influenced more by deep-ocean water-mass properties than thermocline depth, unlike steric height. While steric height changes are usually decomposed into thermosteric and halosteric contributions (e.g., Munk, 2002), here Δh_ρ is also influenced by the pressure loading of meltwater. This effect is hidden in the differing integral limits of equation (15). Seawater contraction due to increased pressure counteracts the expansion due to warming and freshening over the deglaciation.

The vertical integral of $S\rho/\rho_0$ is related to the thickness of salt, h_s, that is dissolved in a column of seawater. Although salt may be close to conserved globally, spatial redistributions yield locally nonzero values of Δh_s. The additional mass of salt would cause local sea-level rise without any addition of meltwater. If salt is added over the deglaciation, then Δh_s and the bias have a positive sign, and salt accounts for some of the deglacial sea-level rise. Note that salt also affects seawater density, where sea-level drop due to the contraction of seawater by salinification partially compensates the sea-level rise due to additional mass. In summary, the key equations used to estimate deglacial sea-level rise are (13), (14), and (15).

2.4. LGM reconstructions

For our primary calculations, we use a global gridded reconstruction of LGM temperature and salinity derived by combining a transient ocean circulation model with paleoceanographic observations (Gebbie, 2012, hereafter, G12). We define the LGM to be at the time of the coldest mean oceanic temperature and highest mean seawater oxygen-isotope ratio, $\delta^{18}O_w$, which is 18,000 yr before present in this dataset. Observational constraints include the MARGO project LGM sea surface temperature (Kucera et al., 2006; Waelbroeck et al., 2009), abyssal temperature and salinity derived from four porewater measurements (Adkins et al., 2002), and timeseries of benthic foraminiferal $\delta^{18}O$ in the deep Atlantic and Pacific (Skinner and Shackleton, 2005). In addition, this estimate is fully transient with a time evolution such that it leads to the modern-day temperature and salinity climatology of the World Ocean Circulation Experiment (Gouretski and Koltermann, 2004). The reconstruction is gridded with $4^\circ \times 4^\circ$ horizontal resolution and 33 vertical levels with enhanced upper-ocean resolution of 8 levels in the upper 130 m. Glacial ocean computations are undertaken on the same grid, but the sea-level drop is assumed to be 130 m as indicated by far-field estimates. As sea level is assumed to rise uniformly, changes in ocean circulation (e.g., Wunsch and Stammer, 1998), visco-elastic effects of the solid Earth (e.g., Mitrovica and Peltier, 1991), and gravitational self-attraction of ice sheets (e.g., Kopp et al., 2015) are omitted.

The G12 reconstruction produced estimates of potential temperature, θ, and the oxygen-isotope ratio of seawater, $\delta^{18}O_w$, that are converted here to Conservative Temperature and Absolute Salinity for use with the thermodynamic equation of state (IOC, SCOR, and IAPSO, 2010). The calculations (see Appendix B) assume that global-mean $\delta^{18}O_w$ reflects the dilution of the ocean, and that spatial variations reflect evaporation, precipitation, and sea-ice processes (Rohling and Bigg, 1998). Many of the uncertainties in glacial salinity (Schmidt, 1999; Rohling, 2007), however, are unresolved here. The LGM temperature estimate is also uncertain due to the sparsity of the proxy data. For these reasons, we refer to the LGM reconstruction as Scenario G12. Later in this work, we introduce three other glacial scenarios in order to determine the sensitivity of our findings.

At every location on the 3D grid, we use the thermodynamic equation of state to diagnose ρ_m, ρ_g, $\tilde{\rho}_m$, and $\tilde{\rho}_g$ (IOC, SCOR, and IAPSO, 2010) for the glacial reconstructions and a modern reconstruction based on World Ocean Circulation Experiment climatology (Gouretski and Koltermann, 2004). Here the reference density

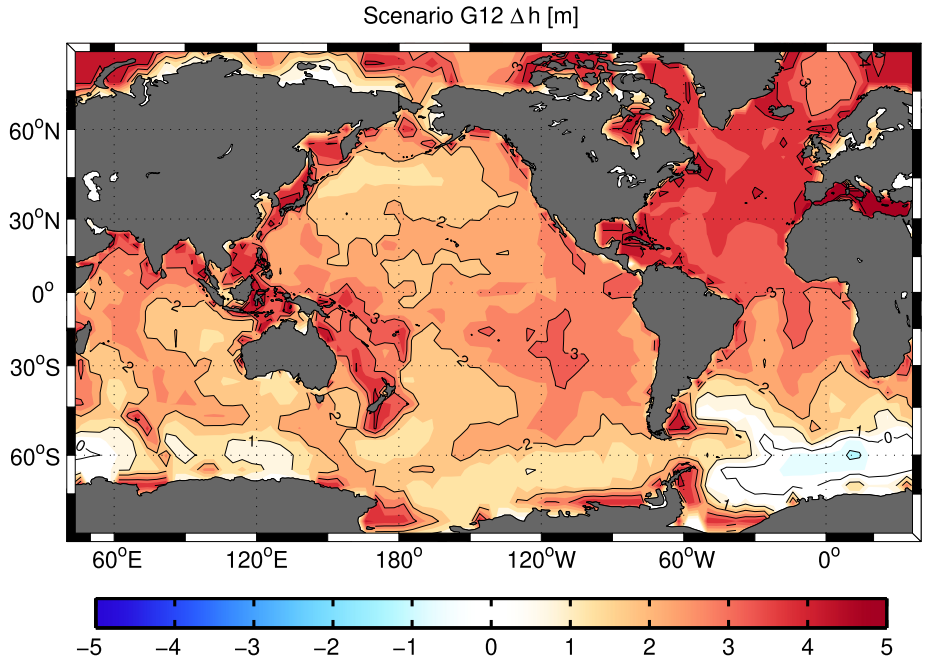

Fig. 1. Column-integrated contribution, $\Delta h(x, y)$, to the bias in inferred ice loss, as diagnosed from LGM scenario G12. The area-weighted average of this field yields the difference between global sea-level rise and the inferred ice loss: 2.6 m.

is defined as IAPSO standard seawater (Culkin and Ridout, 1998) of $\rho_0 = 1026.0$ kg/m^3 (i.e., Absolute Salinity: $S = 35.156$ g/kg, Conservative Temperature: $\Theta = 15.0\,^\circ$C). This choice closely follows the reference density used in multiple glaciological works (e.g., Lambeck and Chappell, 2001; Maris et al., 2014; Patton et al., 2016). Later we test using freshwater as an alternative reference density.

3. Results

3.1. Deglacial ice loss scenario

The contribution to bias in ice-loss estimates is diagnosed in each water column of Scenario G12 according to equation (14). The column-integrated bias, $\Delta h(x, y)$, exceeds 4 m in the Mediterranean Sea and many shallow shelf waters (Fig. 1). The bias is positive almost everywhere in the global ocean, except in the Atlantic sector of the Southern Ocean, which will be investigated later. With the convention used here (i.e., equation (11)), the positive bias indicates that ice-loss estimates, $\Delta\eta_{ice}$, are smaller than the true sea-level rise, $\Delta\eta$.

The spatial pattern of $\Delta h(x, y)$ in Fig. 1 is strongly influenced by deglacial water-mass changes and the seafloor depth, but bears little resemblance to the deglacial change in steric height that instead shows changes in the location and strength of the oceanic gyre circulations (not shown). Recall that $\Delta h(x, y)$ should not be viewed as a map of local sea-level rise, but instead of regional contributions to the bias in global sea level.

The amount of deglacial ice loss necessary to balance the oceanic freshwater budget is diagnosed as the area-weighted average of $\Delta h(x, y)$ from equation (13). The resulting global bias of $B = 2.6$ m indicates that the necessary ice loss is 2.6 m less than the true sea-level rise. For a deglacial sea-level rise of 130.0 m, 127.4 m of ice loss is therefore necessary to balance the freshwater budget. The area-average bias of 2.6 m is somewhat smaller than the 3 m seen in the North Atlantic due to compensating small values in the Southern Ocean and elsewhere.

3.2. Bias from seawater density change

As salt is nearly conserved over the deglaciation, the bias in ice loss estimates must be dominated by the seawater density effect. This density effect, Δh_ρ, has a range from -1 to 5 m that is similar to that from Δh (Fig. 2). When taking the area-weighted average of the Δh_ρ field, we find that the global effect is 2.5 m, confirming its dominant influence on the global-mean bias of 2.6 m diagnosed above.

The global-mean height change due to seawater density, $\overline{\Delta h_\rho}$, is primarily a consequence of a large-scale hydrographic shift. Consider the case that the modern ocean is a two-layer system with a density, $\overline{\rho_{lid}}$, above LGM sea level and $\overline{\rho_{int}}$ below LGM sea level, where the overbar represents a global average in this layer. The descriptor, "lid," refers to the layer above LGM sea level (i.e., meltwater lid) and "int" refers to the ocean below LGM sea level (i.e., the interior). If the LGM ocean is treated as homogeneous with density, $\overline{\rho_g}$, then the first equation in (15) reduces to,

$$\overline{\Delta h_\rho} = -\overline{h_g}\frac{\overline{\Delta\rho}}{\rho_0} \tag{16}$$

where we define $\overline{\Delta\rho} = \overline{\rho_{int}} - \overline{\rho_g}$, we assume that $\rho_{lid} \approx \rho_0$ so that no contribution arises from above LGM sea level, and $\overline{h_g}$ is average depth of the LGM (or interior) ocean. Even though both the LGM and modern seawater density appear very similar and increase by about 30 kg/m^3 from the surface to the abyss (Fig. 3), the modern density is offset by about -0.7 kg/m^3 relative to the LGM (Fig. 4). Substituting representative parameters into (16), we predict a density effect of 2.8 m ($[4 \times 10^3$ m$] \times [7 \times 10^{-1}$ kg/m$^3]/[10^3$ kg/m$^3]$), similar to the full calculation yielding 2.5 m above.

To determine the relative influence of temperature and salinity change, we approximate the deglacial change in density by a linear equation of state,

$$\overline{\Delta\rho} \approx \rho_0[-\alpha\overline{\Delta\Theta} + \beta\overline{\Delta S} + \gamma\overline{\Delta p}], \tag{17}$$

where $\overline{\Delta\Theta}$, $\overline{\Delta S}$, and $\overline{\Delta p}$ are the global-average pointwise changes in temperature, salinity, and pressure between the LGM and the

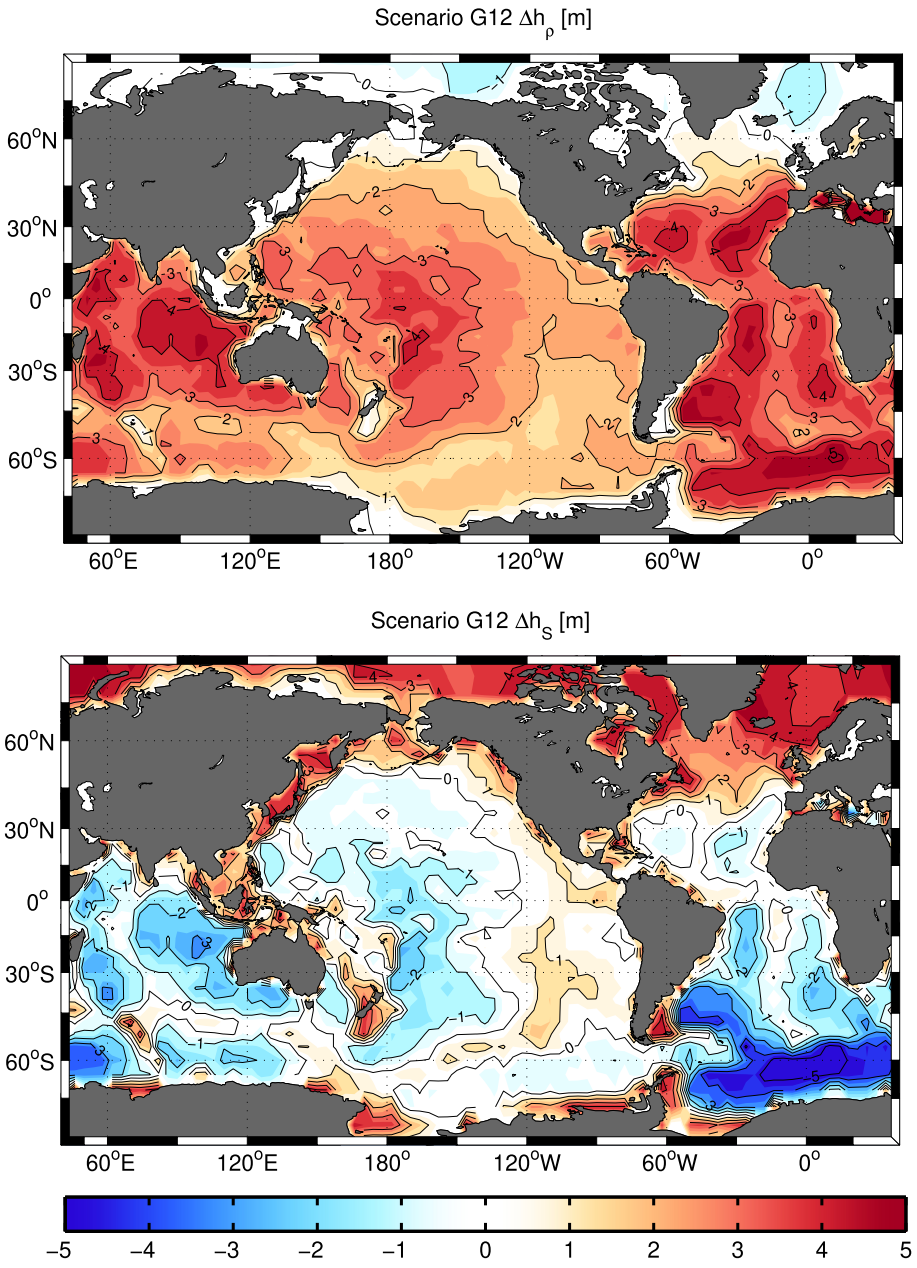

Fig. 2. Column-integrated contributions to the bias in ice-loss estimates from (*top panel*) changes in seawater density, $\Delta h_\rho(x, y)$, and (*bottom panel*) changes in the salt inventory, Δh_s. The contour interval is 1 m.

interior modern ocean at the same location. The coefficients of thermal expansion, haline contraction, and compressibility are α, β, and γ, respectively. The global-mean temperature profile in G12 has a similar structure as the modern day, but with a more homogeneous deep ocean that approaches the freezing point of seawater (*top left*, Fig. 3). The inferred deglacial temperature change is an increase of 3 °C in the upper ocean and 2 °C in the abyss (Fig. 4). The G12 global-mean salinity is about 36 g/kg as is expected from the concentration of salt due to loss of freshwater to land ice (*top right*, Fig. 3), and salinity is even higher in Antarctic Bottom Water (AABW) as constrained by porewater data (Adkins et al., 2002). The deglacial salinity decrease is between 1.0 g/kg and 1.4 g/kg when averaged over depth, where mid-depths have the least freshening because of the relative saltiness of modern North Atlantic Deep Water (NADW). By application of the linear equation of state with representative values (i.e., $\rho_0 = 10^3$ kg/m^3, $\alpha = 1 \times 10^{-4}$ (°C)$^{-1}$, $\overline{\Delta\Theta} = 3$ °C, $\beta = 7 \times 10^{-4}$ kg/g, $\overline{\Delta S} = -1.2$ g/kg, $\gamma = 4 \times 10^{-6}$ dbar^{-1}, $\overline{\Delta p} = 130$ dbar), we estimate that temperature and salinity act to expand seawater by 0.3 and 0.9 kg/m^3, respectively, while the additional pressure load of meltwater contracts seawater by 0.5 kg/m^3. These contributions combine to yield a density change of $\overline{\Delta\rho} = -0.7$ kg/m^3 that agrees with the lower left panel of Fig. 4.

Deglacial freshening is the largest contributor to the density effect and bias in ice-loss estimates, yet the halosteric effect when adding meltwater has been estimated to be vanishingly small (e.g., Lowe and Gregory, 2006). The halosteric effect is indeed small when considering the compensating effects of deglacial freshening below LGM sea level and the salinification of meltwater above LGM sea level. The equivalent sea-level metric, however, uses a baseline density that renders the density effect above LGM sea level small (recall equation (16)), and only the freshening effect from below LGM sea level remains. Because the salinity effect does not vanish in our analysis, we do not refer to a "halosteric" or "thermosteric"

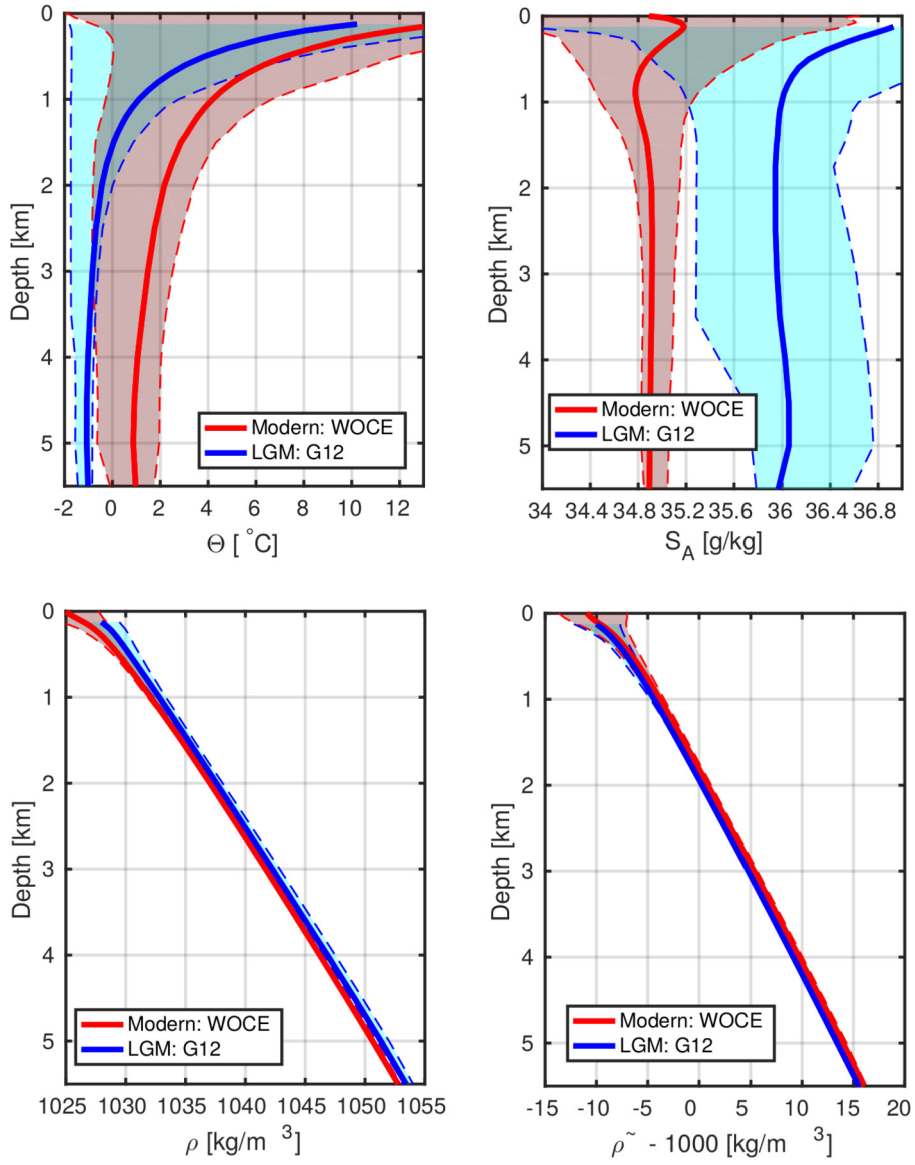

Fig. 3. Global-mean modern (*red line*) and LGM (*blue line*) depth profiles for (*top left*) Conservative Temperature, (*top right*) Absolute Salinity, (*bottom left*) seawater density, and (*bottom right*) freshwater content (offset by 1000 kg/m^3). The shaded range indicates the 5th and 95th percentiles of the spatial variability for modern (*red dashed lines*) and LGM (*blue dashed lines*) distributions. The bottom two panels are magnified in the next figure for better visibility.

effect in this work, as such terms are ambiguous when significant amounts of meltwater are added (e.g., Jordà and Gomis, 2013).

The seawater density effect is not uniformly positive (top panel, Fig. 2), as the highest positive values are over the abyssal plains and smaller values are seen on the continental shelves and mid-oceanic ridges. The regional variations are explained by considering the depth of the ocean, where the density effect is proportional to the ocean depth from equation (16). Negative values in the Arctic are explained by the strong Arctic halocline reconstructed by G12. These fresh LGM surface waters became saltier over the deglaciation in contrast to the global trend. Even in the Arctic subsurface, water freshened an amount, 0.3 g/kg, that is significantly less than the global mean of 1.2 g/kg. Thus the expansion effect by salinity is reduced or eliminated in this region. The remaining pressure effect then dominates and results in deglacial seawater contraction.

3.3. Bias from addition of salt

The spatial field of Δh_s reflects the redistribution of salt over the deglaciation (bottom panel, Fig. 2). The increase of salt in the Arctic and around Antarctica is closely balanced by a decrease in salt elsewhere, such that the area-average of Δh_s is just 1 cm. Accordingly, salt is not perfectly conserved in Scenario G12, as the modern ocean has 0.01% more salt than the LGM, and this salt causes sea level to stand just slightly higher. The effect of Δh_s on the bias in ice-loss estimates is therefore insignificant relative to the density effect.

To understand the spatial pattern of Δh_s, we average the second equation in (15) under the assumption that the modern ocean has two homogeneous layers: the lid and the interior. Defining $\overline{\Delta S} = \overline{S_{int}} - \overline{S_g}$ and assuming $\rho_{lid} \approx \rho_{int} \approx \rho_0$, we obtain an approximate relation,

$$\overline{\Delta h_s} \approx \Delta\eta \overline{S_{lid}} + \overline{h_g}\,\overline{\Delta S}, \tag{18}$$

where the term, $\overline{h_g}\ \overline{S_{int}}\ \overline{\Delta\rho}/\rho_0$, and higher-order terms are neglected because they are at least an order of magnitude smaller. In the global average, the first term is balanced by the second term, as the excavation of salt into the lid is balanced by a freshening in the interior. A similar scaling could be derived for any local

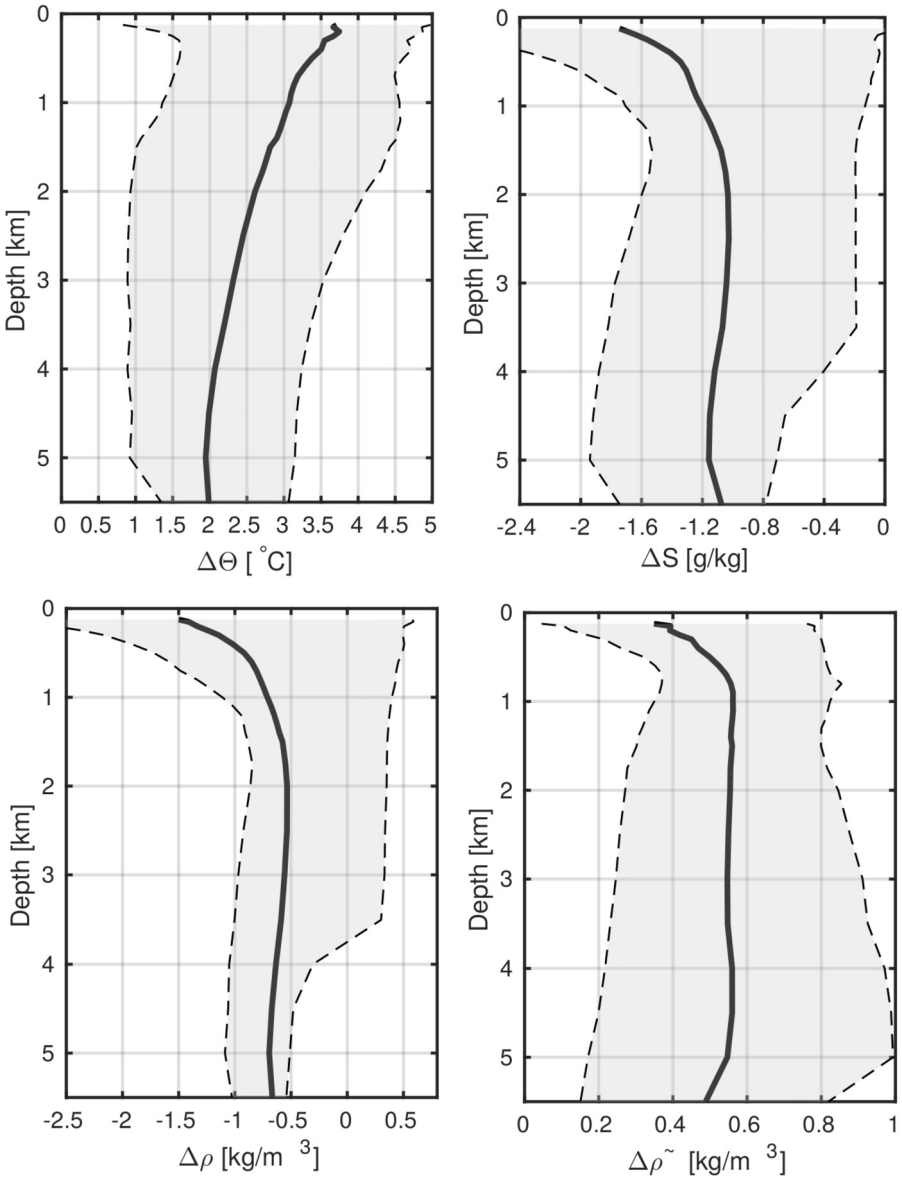

Fig. 4. Depth profile of global-mean modern minus LGM difference (*black lines*) in (*top left*) Conservative Temperature, (*top right*) Absolute Salinity, (*bottom left*) seawater density, and (*bottom right*) freshwater content. The range of values (*gray shading*) represents the 5th and 95th percentiles of the spatial variability.

water column, and here is used to investigate the large negative values in the Weddell Sea. LGM AABW is reconstructed to be as much as 2.0 g/kg saltier than the relatively-fresh modern vintage (e.g., Adkins et al., 2002), implying a large deglacial freshening and relatively-high modern freshwater content. According to the scaling in equation (18), Δh_s is expected to be as negative as -4 m ($[1.3 \times 10^2$ m$] \times [3 \times 10^{-2}$ kg/kg$] + [4 \times 10^3$ m$] \times [-2 \times 10^{-3}$ kg/kg$]$). The scaling is consistent with the equivalent of 5 m of salt that is exported from the Weddell Sea according to G12. A signal of the opposite sense (i.e., $\Delta h_s > 0$) is apparent in the North Atlantic, where relatively less freshening occurred over the deglaciation.

The anticorrelation between the top and bottom panels of Fig. 2 is also explained by investigating salinity. We expand equation (16) using (17) and then add (18) to obtain a relation for the sea-level bias,

$$B \equiv \overline{\Delta h} \approx \Delta\eta \overline{S_{lid}} + \overline{h_g} \left\{ \alpha \overline{\Delta\Theta} + (1-\beta)\overline{\Delta S} - \gamma \overline{\Delta p} \right\}. \tag{19}$$

The sensitivity of $\overline{\Delta h}/\overline{h_g}$ to salinity change is $1-\beta$ and includes two effects. The direct salinity effect of raising sea level by the addition of salt gives the positive sensitivity of 1, and can be tracked through the Δh_s contribution. The indirect salinity effect of haline contraction causes a negative sensitivity of $\beta \approx 0.7$ kg/kg through the density contribution, Δh_ρ. Equation (19) also holds locally so long as the averages are defined over a water column. The local competition between the two salinity effects gives rise to the anticorrelation in the spatial patterns of Δh_s and Δh_ρ (Fig. 2).

4. Discussion

4.1. Comparison of LGM scenarios

The G12 temperature and salinity reconstruction is highly underconstrained by data. The sensitivity of the results in Section 3 is analyzed through three additional LGM reconstructions that are constrained by differing combinations of data (Table 1). Scenario G14 is the primary solution of Gebbie (2014), and primarily uses Atlantic benthic foraminiferal data of δ^{13}C, δ^{18}O, and Cd data, but the porewater data is omitted. The alternate solution from that work (hereafter, G14A), is identical but restricts δ^{13}C to be no more

Table 1
LGM scenarios. Scenarios are derived from a transient model (*checkmark in column 2*) or equilibrium model (*"X" in column 2*). Columns 3 – 7 indicate the number of observations for each data type: MARGO sea surface temperature (*column 3*), porewater data (*column 4*), benthic foraminiferal δ^{18}O (*column 5*), benthic foraminiferal δ^{13}C (*column 6*), and benthic foraminiferal Cd/Ca (*column 7*). The original reference for each reconstruction is given under *Reference*.

Name	Transient	MARGO SST	Porewater	δ^{18}O	δ^{13}C	Cd/Ca	Reference
G12	✓	2806	4	2	0	0	Gebbie (2012)
G14	×	2806	0	241	174	87	Gebbie (2014)
G14A	×	2806	0	241	174	87	Gebbie (2014)
GPLS2	×	2806	0	492	492	0	Gebbie et al. (2015)

depleted than −0.2‰ in an attempt to gauge the potential influence of the Mackensen et al. (2000) effect. Scenario GPLS2 is the secondary solution from Gebbie et al. (2015) and is constrained with a global compilation of over 400 δ^{18}O and δ^{13}C data points, but does not include Cd or porewater data. The primary solution from that work (hereafter, GPLS1) is not used because there was an unreasonably large deglacial sink of 1.7% of oceanic salt. Of the four LGM solutions, only G14A has NADW that is shoaled relative to the modern day, and only Scenario G14 has a significantly increased amount of accumulated remineralized phosphate in the deep Atlantic.

The lack of agreement in the global-mean profile of LGM-to-modern density change clearly illustrates the remaining uncertainty amongst the four LGM reconstructions (Fig. 5). In the upper ocean, the estimated density change varies by a factor of 4, between −0.3 kg/m^3 and −1.2 kg/m^3. In the deep ocean, variations on the order of 25% exist. In addition, the vertical structure of density is not consistent, as two inversions have a generally monotonic change with depth (G14, G14A), and two do not. Similar deviations exist in the vertical structure of freshwater content. The freshwater content has a smaller deglacial increase according to G12 relative to the other reconstructions.

The range of freshwater changes can be traced back to uncertainties in the LGM temperature and salinity fields. The estimated range of surface temperature change is from 1 °C to 3 °C, and the global-mean temperature change has a similarly large range. Heavy noble gas measurements from bubbles trapped in WAIS Divide ice sheet suggest a global-mean oceanic temperature change of 2.6 °C (Bereiter et al., 2018), within our range of reconstructions. The global-mean salinity change is expected to be near −1.17 g/kg due to dilution by meltwater without any deglacial warming, and −1.15 g/kg with a deglacial warming of 2.5 °C (Appendix C). In addition, the reconstructions permit small amounts of salt to be added or removed during the flooding of the continental shelves. More specifically, the deglacial change in salt inventory is 0.01%, 0.07%, −0.03%, and −0.32% of the modern inventory, for G12, G14, G14A, and GPLS2, respectively. The resulting global-mean salinity change is −1.14, −1.12, −1.15, and −1.26 g/kg, indicating some remaining uncertainty. The freshwater content is better correlated with salinity change rather than density change, in agreement with the $\overline{\Delta S}$ coefficient in equation (19).

Despite wide variations in temperature and salinity between the four reconstructions, there is general agreement in the regional pattens, $\Delta h(x, y)$, of the depth-integrated ice-loss bias (Fig. 6). All scenarios are dominated by positive values up to 5 m. Some of the spatial patterns are consistent as would be expected due to bathymetric features, such as the relatively low bias due to the decreased water depth above the Mid-Atlantic Ridge and East Pacific Rise. The area-averaged bias, B, is 2.6, 2.4, 2.1, and 2.0 m in the four reconstructions. Thus, the ice loss needed to explain the deglaciation is 127.4, 127.6, 127.9, and 128.0 m of sea-level equivalent in scenarios G12, G14, G14A, and GPLS2, respectively. All scenarios suggest that less ice is needed than the assumed true sea-level rise of 130.0 m (Table 2).

4.2. Dependence on global mean changes

While many regional variations exist and the equation of state is nonlinear, we hypothesize that the differences between the four scenarios can be explained by global-mean temperature and salinity changes. We next test the skill of the following relationship,

$$B \approx a_1 \overline{\Delta\Theta} + a_2 \overline{\Delta S} + a_3, \tag{20}$$

where a_1, a_2 and a_3 are regression coefficients, and $\overline{\Delta\Theta}$ and $\overline{\Delta S}$ are the average Conservative Temperature and Absolute Salinity change below LGM sea level. We compute $\overline{\Delta\Theta}$ and $\overline{\Delta S}$ by differencing the LGM and modern properties at the same location, and then taking the average. Thus, the modern ocean above 130 m depth is not considered because it has no LGM analog. Given the four deglacial scenarios, we have four independent constraints on the three unknown coefficients, a_1, a_2, and a_3. Using an ordinary least squares method, we find $a_1 = (0.5 \pm 0.1)$ m/°C, $a_2 = (0.8 \pm 0.6)$ m/(g/kg), and $a_3 = (2.2 \pm 0.8)$ m. Equation (20) with the a_1, a_2, and a_3 coefficients reproduces the complete 3D analysis with a root-mean-square error of less than 1 cm (Fig. 7). Thus, global-mean hydrographic shifts are the dominant driver of biases in inferred ice loss.

The empirically-derived coefficients are consistent in sign and magnitude with those expected from the equation of state. From equation (19), we have a scaling for B. Assuming an average thermal expansion coefficient of $\alpha = 1 \times 10^{-4}$ (°C)$^{-1}$ and a typical haline contraction coefficient of $\beta = 7 \times 10^{-4}$ (kg/g), substitution into (19) predicts a value of $a_1 = 0.42$ m/°C and $a_2 = 1.16$ m/(g/kg) that are consistent with the regression results. The value of a_3 is set by the sum of two terms. Substituting $\gamma = 4 \times 10^{-6}$ dbar^{-1} and $\overline{\Delta p} = 130$ dbar yields a contribution of $-\overline{h_g}\gamma\overline{\Delta p} = -2.0$ m to a_3 from below LGM sea level. Above LGM sea level we substitute $\Delta\eta = 130$ m and $\overline{S_{lid}} = 0.035$ kg/kg to find a bias of $\Delta\eta\overline{S_{lid}} = 4.5$ m. Combining the two, we find a final predicted value of $a_3 = 2.5$ m that is also consistent with the regression coefficient.

The regression coefficient, a_1, gives the sensitivity of the bias to the LGM-to-modern temperature change. The value of $a_1 = (0.5 \pm 0.1)$ m/°C is specific to the long-term evolution of the deglaciation that permits deep ocean adjustment. A related quantity is the thermal expansion sensitivity, which has been diagnosed from steric height changes as 0.13 m/°C in 20th Century observations (Bindoff et al., 2007) and 0.17 m/°C from climate models of the last interglacial (McKay et al., 2011). These studies likely have smaller values because of their focus on the upper 700 m only. The thermal expansion effect that includes deep ocean adjustment is uncertain but likely larger and in the range of 0.2–0.6 m/°C (Meehl et al., 2007). Our estimate of the bias sensitivity is within this range, although near the upper end.

4.3. Other deglacial temperature change estimates

Our four scenarios of LGM temperature and salinity may not represent the true range of uncertainty. Here we use the regression results of the previous section to assess the uncertainty

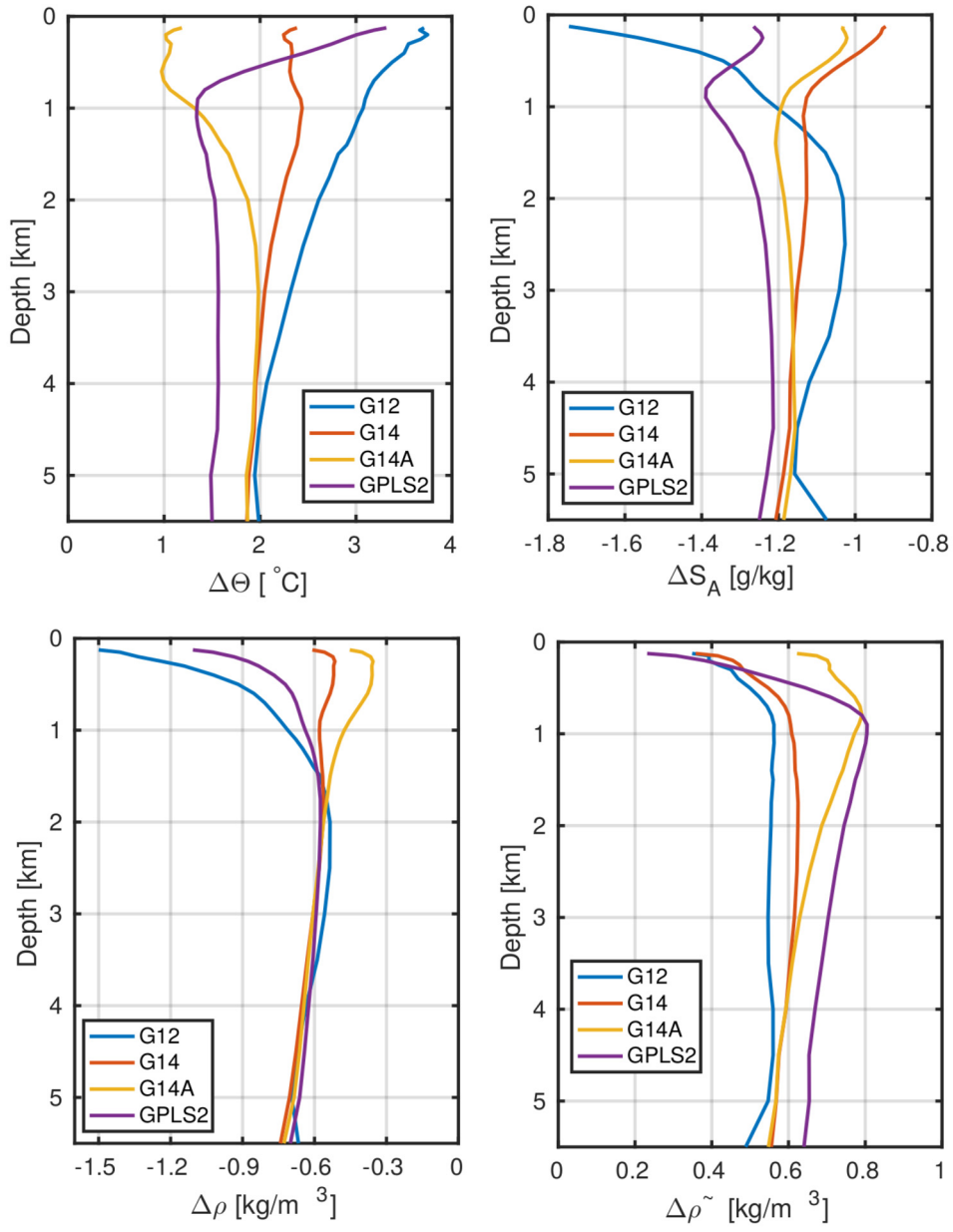

Fig. 5. Depth profile of global-mean modern minus LGM difference in (*top left*) Conservative Temperature, (*top right*) Absolute Salinity, (*bottom left*) density, and (*bottom right*) freshwater content. The differences are plotted for four scenarios: G12 (*blue*), G14 (*red*), G14A (*yellow*), and GPLS2 (*purple*).

with independent information. Assuming that salt is conserved as computed in Appendix C, temperature information is sufficient to make an estimate of the bias. Collapsing Fig. 7 along the line where salt is conserved (i.e., $\Delta S = \Delta S_{cons}$) yields a relation for B that solely depends on temperature change (Fig. 8). Deep-ocean foraminiferal oxygen isotopic ratios suggest a temperature change of $\overline{\Theta_m} - \overline{\Theta_g} = 3.0 \pm 1.0\,^{\circ}\mathrm{C}$ (Elderfield et al., 2012), but this temperature difference is computed differently than our regression analysis. To find the global-average change below LGM sea level consistent with the regression equation, a shift of $-0.4\,^{\circ}\mathrm{C}$ must be applied. Applying a temperature change of $\overline{\Delta\Theta} = 2.6 \pm 1.0\,^{\circ}\mathrm{C}$, we estimate that the necessary ice loss was 127.4 ± 0.5 m when propagating the uncertainties in the temperature and regression coefficients. Thus the bias is 2.6 ± 0.5 m less than the assumed 130 m of sea-level rise. A recent estimate of global-mean temperature change from heavy noble gas measurements in ice sheet bubbles is $\overline{\Theta_m} - \overline{\Theta_g} = (2.57 \pm 0.24)\,^{\circ}\mathrm{C}$ (Bereiter et al., 2018), which gives a pointwise difference of $\overline{\Delta\Theta} = (2.17 \pm 0.24)\,^{\circ}\mathrm{C}$ below LGM sea level. The bias then has a similar central estimate but with smaller error bars: $B = 2.33 \pm 0.13$ m.

The deglacial salt budget is unlikely to be perfectly conserved due to the dynamics of sediment exchange, riverine transport, and the carbon cycle. Also, global-mean salinity changes can occur due to changes in sea ice, yet these do not change the net amount of salt. To account for these processes, the four reconstructions were not constrained to conserve salt perfectly. If deglacial flooding exhumes salt from the continental shelves, then sea level rises due to the addition of the mass of salt, but seawater contracts due to the increased salinity. Both effects are of the same order, but the positive coefficient, a_2, indicates that the direct effect due to the mass of salt wins out. If the global-mean salinity field is not constrained better than ± 0.2 g/kg, the salt budget therefore incurs an additional uncertainty, leading to a bias of 2.33 ± 0.21 m when using the Bereiter et al. (2018) deglacial warming estimate. When using the Elderfield et al. (2012) estimate, on the other hand, the

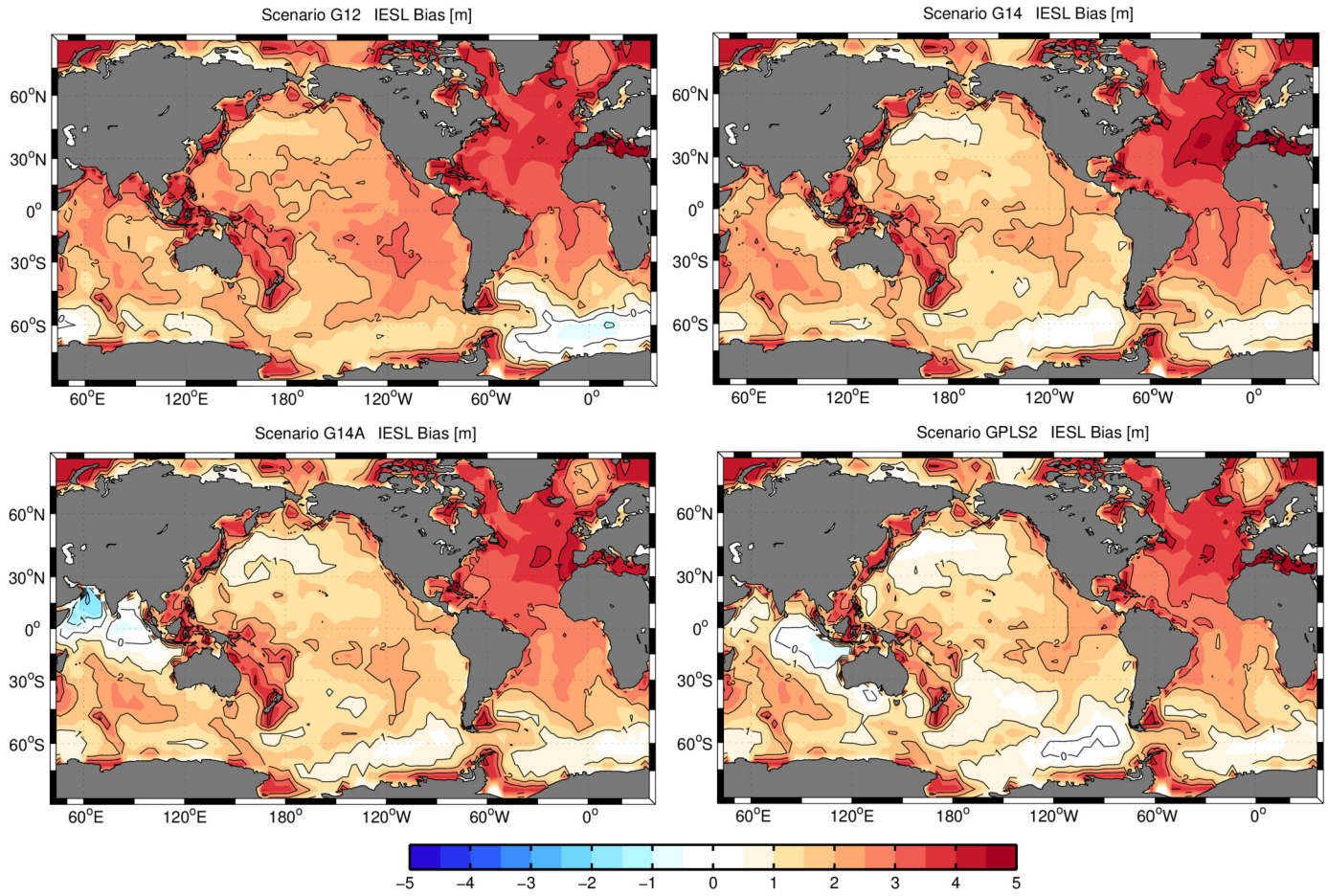

Fig. 6. Column-integrated contributions to the bias in ice-loss estimates calculated from four reconstructions: G12 (*top left*), G14 (*top right*), G14A (*bottom left*), and GPLS2 (*bottom right*).

Table 2
LGM-to-modern global mean of Conservative Temperature pointwise difference (*column 2*, computed as the modern interior minus glacial values), difference of global mean Conservative Temperature (*column 3*), mean pointwise-difference of Absolute Salinity (*column 4*), difference of mean Absolute Salinity (*column 5*), estimated ice loss in equivalent sea level (*column 6*), and difference between sea-level rise and ice loss (*column 7*), as estimated in four LGM reconstructions (*column 1*): G12, G14, G14A, and GPLS2.

LGM Scenario	$\overline{\Delta\Theta}$ [°C]	$\overline{\Theta_m} - \overline{\Theta_g}$ [°C]	$\overline{\Delta S}$ [g/kg]	$\overline{S_m} - \overline{S_g}$ [g/kg]	$\Delta\eta_{ice}$ [m]	B [m]
G12	2.62	3.03	−1.14	−1.13	127.4	2.6
G14	2.17	2.57	−1.12	−1.12	127.6	2.4
G14A	1.69	2.09	−1.16	−1.15	127.9	2.1
GPLS2	1.63	2.03	−1.26	−1.26	128.0	2.0

inferred bias and error bars are not significantly changed due to the already-existing large uncertainty from temperature.

4.4. Physical mechanisms leading to bias

When meltwater is added but mean ocean temperature doesn't change, the regression suggests that the inferred ice loss would still be biased low. The salinity change for 130 m of sea-level rise is $\overline{\Delta S} = -1.17$ g/kg due to dilution. Substituting into the regression of equation (20), we find that the bias is 1.2 m. As temperature doesn't change in this case, the bias must arise from other factors.

To identify the physical mechanisms behind the bias, the regression equation (20) must be modified to relax the assumption of a sea-level rise of 130 m. In the modern ocean, the mass of salt above LGM sea level, $\Delta\eta\overline{S_{lid}}$, displaces freshwater and contributes to the ice-loss bias. This bias is compensated below LGM sea level, however, by a loss of salt with mass, $\overline{h_g}\ \overline{\Delta S}$. When salt is conserved over the deglaciation, these two effects are balanced. Eliminating these canceling terms, equation (19) reduces to,

$$B_{cons} \approx \Delta\eta \left\{ \beta\, \overline{S_{int}} - \gamma\ P\, \overline{h_g} \right\}, \tag{21}$$

where P is the conversion factor from meters of sea level to pressure in decibars, and the following assumptions are made: $\overline{\Delta\Theta} = 0$, $\overline{\Delta S} = -\overline{S_{lid}}\Delta\eta/\overline{h_g}$, and $\overline{\Delta p} = P\Delta\eta$. For any meltwater added to the ocean (i.e., $\Delta\eta \neq 0$), a bias will be incurred unless the salinity and pressure terms in the curly brackets of (21) balance. This balance depends upon quantities that are available in the modern ocean, where we find that the salinity term wins out ($[7 \times 10^{-4}$ kg/g$] \times [35$ g/kg$] = 2.4 \times 10^{-2}$) over the pressure term ($[4 \times 10^{-6}$ dbar$^{-1}] \times [1$ dbar/m$] \times [4 \times 10^{3}$ m$] = 1.6 \times 10^{-2}$). As these parameters are well constrained, this analysis predicts that any addition of meltwater will lead to a positive bias.

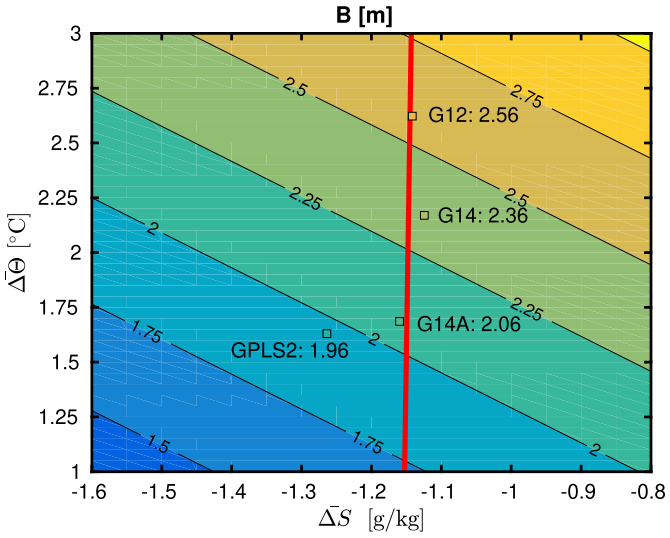

Fig. 7. The ice-loss bias as a function of the modern-minus-LGM difference in mean temperature ($\overline{\Delta\Theta}$, *y-axis*) and salinity ($\overline{\Delta S}$, *x-axis*) below LGM sea level. The diagnostics from four LGM scenarios (*open symbols, text values of bias*) are placed in the context of a multiple linear regression model (*background colors and contours*). The case where salt is conserved and salinity is well mixed is emphasized (*red line*). (For interpretation of the colors in the figure(s), the reader is referred to the web version of this article.)

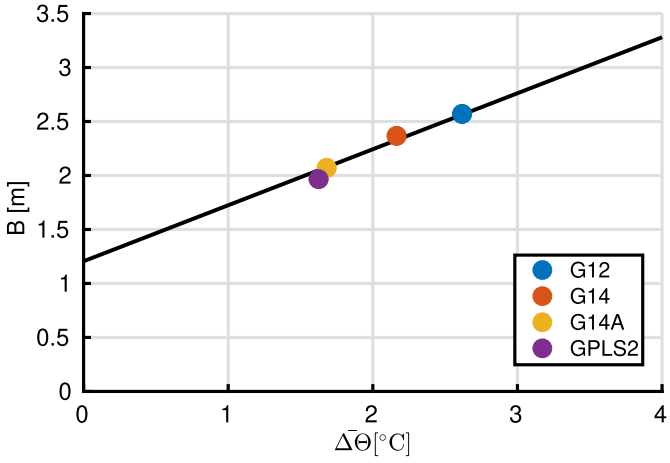

Fig. 8. The ice-loss bias as a function of the modern-minus-LGM difference in mean temperature below LGM sea level ($\overline{\Delta\Theta}$, *x-axis*) in a case where salt is perfectly conserved. The biases from four LGM scenarios are included. The thick black line is the regression equation for B, where deviations from the line occur in part due to the imperfect conservation of salt (*symbols*).

All of the preceding analysis follows from a consideration of the distribution of freshwater content, $\tilde{\rho}$. Even though the LGM ocean was at a higher density than the modern at all depths where both oceans existed, the relationship is reversed when considering the freshwater content (*bottom panel*, Fig. 4). Instead, freshwater content increased over the deglaciation. A seemingly-natural conclusion is that even more ice melt must be added to the deglacial ocean to provide the increased freshwater content, but this addition is compensated by a flux of salt into waters above LGM sea level. What remains is the effect of seawater density on freshwater content changes. Below LGM sea level, deglacial freshening causes expansion that exceeds the contraction due to the additional pressure loading of meltwater. This competition explains the results of the scaling argument in the previous paragraph. Any deglacial warming will augment the expansion due to freshening. Together the temperature and salinity effects require less deglacial ice loss to explain a given rise in sea level.

4.5. Modifying the definition of sealevel equivalent

Ice-loss estimates are easily modified by replacing the baseline seawater density, ρ_0, with the density of freshwater. The use of freshwater density causes the ice-loss estimate, $\Delta\eta_{ice}$, to be about 3% greater due to the denominator in equation (8). In this case, $\Delta\eta_{ice}$ almost always exceeds $\Delta\eta$ and the bias is negative. Therefore, using $\rho_0 = 1000$ kg/m^3 also leads to a bias, but one where ice-loss estimates would be too large. There is no choice of reference density that eliminates bias in all cases.

5. Conclusion

Estimates of ice loss over the deglaciation do not appear to account for the full sea-level rise as inferred from far-field techniques, but up to three meters of the discrepancy can be explained as an artifact of expressing ice loss in terms of sea level equivalent. The difference between ice-loss estimates and actual sea-level rise occurs due to the changing distribution of freshwater during the deglaciation. Here we use four reconstructions of LGM temperature and salinity to put bounds on what this freshwater content change might have been. For a true deglacial sea-level rise assumed to be 130 m, four LGM reconstructions bracket the ice loss to a range of 127.4 to 128.0 m. Independent estimates of temperature change suggest that the plausible range may be as large as 127.4 ± 0.5 m. Despite remaining uncertainties in the spatial structure of freshwater content change, the sign of the effect on global-mean sea level is robust in all cases examined here.

Deglacial changes in freshwater content are affected by both the seawater salinity and density. While salinity changes imply that both the mass and the seawater density are changed, the seawater equation of state determines that the mass effect is most important for local sea level. Although deglacial salinity changes are large, there is a global balance between the salt lost below LGM sea level and that gained above LGM sea level. Thus, the salinity effect on freshwater content nearly cancels in the global average, such that the remaining seawater density effect is most important for determining the amount of deglacial ice loss. Expansion of seawater requires less ice loss for a given sea-level rise.

For any period of sea-level rise, there is a built-in tendency for an ice-loss estimate inferred from ocean changes to be biased low. Over the deglaciation, for example, the ocean below LGM sea level freshens due to dilution but is subject to a greater pressure due to meltwater loading. The haline expansion outweighs the compression by the pressure effect. Even without any deglacial ocean warming, the ice-loss estimate inferred from ocean properties would be biased low relative to the true sea-level rise. This bias is intrinsic to the expression of ice loss in terms of equivalent sea-level rise. When deglacial temperature rise is also taken into account, seawater further expands and therefore the bias in the inferred ice loss is even larger.

How could the definition of sea level equivalent be refined to eliminate the bias? The description of ice loss in terms of its most basic unit, kilograms, is advisable, but this requires a careful reanalysis of the glaciological literature. In addition, it is often helpful to provide an approximate sea level equivalent, so it is difficult to envision a future where this term is completely eliminated. For ice mass to be translated into sea-level rise accurately, knowledge of density, the timing of oceanic meltwater input, and the hypsometry of the seafloor are key and cannot be avoided. One way forward is to retain the conventional definition of equivalent sea level, and to use the regression analysis of this work to correct for the bias over the last deglaciation. A different correction may have to be applied to meltwater addition in the modern ocean, however, as modern warming has had less time to penetrate to depth. Ultimately, we expect that an adjustment of existing ice loss estimates

will reduce the amount of missing LGM ice, although it appears that some discrepancy with far-field sea-level rise estimates still remains (e.g., Simms et al., 2019).

Acknowledgements

We thank Olivier Marchal for a thorough review of the mathematics, and we thank Magdalena Andres, Markus Kienast, Chris Piecuch, Zan Stine, and the students of MIT/WHOI 12.808, *Introduction to Observational Physical Oceanography*, for discussions. GG is funded by NSF OCE-1536380.

Appendix A. Deglacial-average ocean area

The deglacial change in ocean volume is,

$$\Delta V \equiv \int_{Z_g}^{Z_m}\int^{X}\int^{Y} dy\, dx\, dz = \int_{Z_g}^{Z_m} A(z)\, dz, \tag{A.1}$$

where the horizontal area of the ocean is a function of the vertical coordinate, $A(z)$. In our case, the volume change is calculated assuming the sea-level change of 130 m (i.e., $\Delta\eta \equiv Z_m - Z_g = 130$ m). Here we define A_{dg} such that it gives the true deglacial volume change:

$$\Delta V \equiv \int_{Z_g}^{Z_m} A_{dg}\, dz. \tag{A.2}$$

Rearranging this equation yields,

$$A_{dg} \equiv \frac{\Delta V}{\Delta\eta} = \frac{1}{\Delta\eta}\int_{Z_g}^{Z_m}\int^{X}\int^{Y} dy\, dx\, dz, \tag{A.3}$$

where the deglacial-average area is equal to the oceanic volume above LGM sea level divided by the sea-level rise, $\Delta\eta$. This definition is only valid in cases where the sea-level changes.

Appendix B. Inputs to the thermodynamic equation of state

Scenario G12 $\delta^{18}O_w$ is translated to Absolute Salinity for use with the 2010 thermodynamic equation of state. Changes in mean-ocean $\delta^{18}O_w$ are assumed to reflect dilution by meltwater, and the G12 estimate of a global-mean LGM-to-modern $\delta^{18}O_w$ change of -1.03‰ is scaled to a global-mean salinity change. To obtain the scaling coefficient, we take the unbiased estimate of salinity change from Appendix C: -1.17 g/kg.

Spatial variations in $\delta^{18}O_w$ and salinity are due to evaporation, precipitation, and sea-ice processes that are distinct from the global dilution signal (e.g., Rohling and Bigg, 1998). The porewater data (Adkins et al., 2002) is best fit with a linear relationship where the ratio between salinity and $\delta^{18}O_w$ deviations is 4:1. This ratio is larger than that found in the modern ocean (e.g., Gebbie and Huybers, 2006), which is closer to 2:1 in the subtropical and tropical oceans. Combining the global mean and spatial deviations, the empirical relationship for glacial salinity is,

$$S_g = \overline{S_g} + 4(\delta^{18}O_w]_g - \overline{\delta^{18}O_w]_g}), \tag{B.1}$$

where LGM global-mean salinity is higher than the modern, $\overline{S_g} = \overline{S_m} + 1.17$ g/kg (Appendix C), and similarly for the global-mean oxygen-isotope ratio of seawater, $\overline{\delta^{18}O_w]_g} = \overline{\delta^{18}O_w]_m} + 1.03$‰.

For the reconstructions, G14, G14A, and GPLS2, gridded fields of LGM practical salinity were produced by the original works. To translate to Absolute Salinity, the modern-day lookup table provided by the Gibbs seawater toolbox is not applicable to the glacial ocean, as the carbon cycle was likely in a different state. Instead we use an empirical relationship between phosphate and the non-conservative part of salinity (see Appendix A1, Gebbie et al., 2016) that captures about half of the variance in the carbon cycle effect.

For all reconstructions, Absolute Salinity is first determined. Then, Conservative Temperature is determined from potential temperature and Absolute Salinity using the MATLAB Gibbs seawater toolbox (IOC, SCOR, and IAPSO, 2010).

Appendix C. Salinity change due to dilution

The goal of this appendix is to diagnose the deglacial change in salinity due to dilution from modern quantities. If there is no deglacial source or sink of salt, the salt budget is,

$$\bar{S}_g\mathcal{M}_g = \bar{S}_m\mathcal{M}_m, \tag{C.1}$$

where $\bar{S}_g$ is mean glacial salinity, $\mathcal{M}_g$ is the LGM mass of seawater, $\bar{S}_m$ is mean modern salinity, and $\mathcal{M}_m$ is the modern mass of seawater. Rearranging, the global-mean LGM salinity is,

$$\bar{S}_g = \frac{\mathcal{M}_m}{\mathcal{M}_g}\bar{S}_m. \tag{C.2}$$

In order to better relate to the quantities in the main text, the LGM salinity is further decomposed into contributions from above and below LGM sea level,

$$\bar{S}_g = \frac{1}{\mathcal{M}_g}(\bar{S}_{int}\mathcal{M}_{int} + \bar{S}_{lid}\mathcal{M}_{lid}), \tag{C.3}$$

where $\bar{S}_{int}$ and $\mathcal{M}_{int}$ correspond to quantities below LGM sea level, and $\bar{S}_{lid}$ and $\mathcal{M}_{lid}$ correspond to quantities above LGM sea level. This expression, however, depends on the LGM mass of seawater in addition to modern-day quantities.

With the aim of replacing $\mathcal{M}_g$ with quantities that are better known, we first rearrange equation (1) and split the modern seawater mass into two components to solve for the mass of ice, $\Delta M_{ice} = M_{int} + M_{lid} - M_g$. Using salt conservation to replace the freshwater masses with seawater masses and rearranging, we obtain, $\mathcal{M}_g = \mathcal{M}_{int} + \mathcal{M}_{lid} - \Delta M_{ice}$, where $\Delta\mathcal{M}_{ice} = \Delta M_{ice}$ because it contains no salt. Next, the bias in units of kilograms is defined to be, $\mathcal{B} = B\ \rho_0\ A_{dg} = \mathcal{M}_{lid} - M_{ice}$, where the second equivalence follows from equation (13). Using this expression, the LGM mass of seawater is simplified, $\mathcal{M}_g = \mathcal{M}_{int} + \mathcal{B}$, so that the LGM average salinity is,

$$\bar{S}_g = \frac{1}{\mathcal{M}_{int} + \mathcal{B}}(\bar{S}_{int}\mathcal{M}_{int} + \bar{S}_{lid}\mathcal{M}_{lid}), \tag{C.4}$$

where only modern quantities and one deglacial quantity, the ice-loss bias, $\mathcal{B}$, are required.

An important quantity is the deglacial change in salinity due to dilution as computed by comparing salinity at the same locations, $\Delta S_{cons} = \bar{S}_{int} - \bar{S}_g$. From equation (C.4) we obtain,

$$\Delta S_{cons} = \frac{-\mathcal{M}_{lid}\bar{S}_{lid} + \mathcal{B}\bar{S}_{int}}{\mathcal{M}_{int} + \mathcal{B}}, \tag{C.5}$$

where the label "cons" indicates that salt is conserved over the deglaciation. When the bias vanishes, equation (C.5) is dominated by,

$$\Delta S_{cons} \approx -\bar{S}_{lid}\frac{\mathcal{M}_{lid}}{\mathcal{M}_{int}}, \tag{C.6}$$

the freshening of the ocean due to dilution. The quantities $\bar{S}_{lid}$, $\mathcal{M}_{lid}$, and $\mathcal{M}_m$ are known from the modern-day ocean, and substitution into (C.6) yields a freshening of 1.17 g/kg.

A better estimate of the salinity change includes the bias term. Then, equation (C.5) is actually a nonlinear expression because $\mathcal{B}$ is a function of $\overline{\Delta S}$ and $\overline{\Delta\Theta}$. The effect of the bias is to make the necessary salinity change smaller, both by affecting the numerator and denominator of (C.5). Fortunately, values of ΔS_{cons} are only a slight function of $\overline{\Delta\Theta}$, leading to a decrease in freshening by up to 0.05 g/kg for a large bias of $B = 5$ m.

References

Adkins, J.F., McIntyre, K., Schrag, D.P., 2002. The salinity, temperature, and δ^{18}O of the glacial deep ocean. Science 298 (5599), 1769–1773.

Austermann, J., Mitrovica, J.X., Latychev, K., Milne, G.A., 2013. Barbados-based estimate of ice volume at Last Glacial Maximum affected by subducted plate. Nat. Geosci. 6 (7), 553.

Becker, J., Sandwell, D., Smith, W., Braud, J., Binder, B., Depner, J., Fabre, D., Factor, J., Ingalls, S., Kim, S., et al., 2009. Global bathymetry and elevation data at 30 arc seconds resolution: Srtm30_plus. Mar. Geod. 32 (4), 355–371.

Bereiter, B., Shackleton, S., Baggenstos, D., Kawamura, K., Severinghaus, J., 2018. Mean global ocean temperatures during the last glacial transition. Nature 553 (7686), 39.

Bindoff, N., Willebrand, J., Artale, V., Cazenave, A., Gregory, J., Gulev, S., Hanawa, K., Le Quere, C., Levitus, S., Nojiri, Y., et al., 2007. Observations: oceanic climate and sea level. In: Climate Change 2007: The Physical Science Basis. Contribution of Working Group I to the Fourth Assessment Report of the Intergovernmental Panel on Climate Change. Cambridge University Press, Cambridge, UK, and New York, USA, pp. 385–432.

Clark, P., Dyke, A., Shakun, J., Carlson, A., Clark, J., Wohlfarth, B., Mitrovica, J., Hostetler, S., McCabe, A., 2009. The last glacial maximum. Science 325 (5941), 710–714.

Clark, P.U., Tarasov, L., 2014. Closing the sea level budget at the Last Glacial Maximum. Proc. Natl. Acad. Sci. 111 (45), 15861–15862.

Culkin, F., Ridout, P., 1998. Stability of IAPSO standard seawater. J. Atmos. Ocean. Technol. 15 (4), 1072–1075.

Elderfield, H., Ferretti, P., Greaves, M., Crowhurst, S., McCave, I., Hodell, D., Piotrowski, A., 2012. Evolution of ocean temperature and ice volume through the mid-Pleistocene climate transition. Science 337 (6095), 704–709.

Fairbanks, R.G., 1989. A 17.000 year glacio eustatic sea level record: influence of glacial melting rates on the Younger Dryas event and deep-ocean circulation. Nature 342, 637–642.

Gebbie, G., 2012. Tracer transport timescales and the observed Atlantic-Pacific lag in the timing of the last Termination. Paleoceanography 27, PA3225. https://doi.org/10.1029/2011PA002273.

Gebbie, G., 2014. How much did Glacial North Atlantic Water shoal? Paleoceanography 29 (3), 190–209.

Gebbie, G., Huybers, P., 2006. Meridional circulation during the Last Glacial Maximum explored through a combination of δ^{18}O observations and a geostrophic inverse model. Geochem. Geophys. Geosyst. 7, Q11N07. https://doi.org/10.1029/2006GC001383.

Gebbie, G., Peterson, C.D., Lisiecki, L.E., Spero, H.J., 2015. Global-mean δ^{13}C and its uncertainty in a glacial state estimate. Quat. Sci. Rev. 125.

Gebbie, G., Streletz, G.J., Spero, H.J., 2016. How well would modern-day oceanic property distributions be known with paleoceanographic-like observations? Paleoceanography 31.

Gill, A.E., Niiler, P., 1973. The theory of seasonal variability in the ocean. Deep-Sea Res. 20, 141–177.

Gouretski, V., Koltermann, K., 2004. WOCE Global Hydrographic Climatology. Tech. Rep. 35. Berichte des Bundesamtes für Seeschifffahrt und Hydrographie.

Griffies, S.M., Greatbatch, R.J., 2012. Physical processes that impact the evolution of global mean sea level in ocean climate models. Ocean Model. 51, 37–72.

Hanebuth, T., Stattegger, K., Grootes, P.M., 2000. Rapid flooding of the Sunda Shelf: a late-glacial sea-level record. Science 288 (5468), 1033–1035.

IOC, SCOR, IAPSO, 2010. The International Thermodynamic Equation of Seawater–2010: Calculation and Use of Thermodynamic Properties. Manuals and Guides No. 56 Intergovernmental Oceanographic Commission, UNESCO (English).

Jordà, G., Gomis, D., 2013. On the interpretation of the steric and mass components of sea level variability: the case of the Mediterranean basin. J. Geophys. Res., Oceans 118 (2), 953–963.

Kopp, R.E., Hay, C.C., Little, C.M., Mitrovica, J.X., 2015. Geographic variability of sea-level change. Curr. Clim. Change Rep. 1 (3), 192–204.

Kucera, M., Rosell-Mele, A., Schneider, R., Waelbroeck, C., Weinelte, M., 2006. Multiproxy approach for the reconstruction of the glacial ocean surface (MARGO). Quat. Sci. Rev. 24.

Lambeck, K., Chappell, J., 2001. Sea level change through the last glacial cycle. Science 292 (5517), 679–686.

Lambeck, K., Rouby, H., Purcell, A., Sun, Y., Sambridge, M., 2014. Sea level and global ice volumes from the Last Glacial Maximum to the Holocene. Proc. Natl. Acad. Sci. 111 (43), 15296–15303.

Lowe, J.A., Gregory, J.M., 2006. Understanding projections of sea level rise in a Hadley Centre coupled climate model. J. Geophys. Res., Oceans 111 (C11).

Mackensen, A., Schumacher, S., Radke, J., Schmidt, D., 2000. Microhabitat preferences and stable carbon isotopes of endobenthic foraminifera: clue to quantitative reconstruction of oceanic new production? Mar. Micropaleontol. 40 (3), 233–258.

Maris, M., De Boer, B., Ligtenberg, S., Crucifix, M., Van De Berg, W., Oerlemans, J., 2014. Modelling the evolution of the Antarctic ice sheet since the last interglacial. Cryosphere 8 (4), 1347–1360.

McKay, N.P., Overpeck, J.T., Otto-Bliesner, B.L., 2011. The role of ocean thermal expansion in Last Interglacial sea level rise. Geophys. Res. Lett. 38 (14).

Meehl, G., Stocker, T., Collins, W., Friedlingstein, P., Gaye, A., Gregory, J., Kitoh, A., Knutti, R., Murphy, J., Noda, A., Raper, S., Watterson, I., Weaver, A., Zhao, Z.-C., 2007. Global climate projections. In: Solomon, S., Qin, D., Manning, M., Chen, Z., Marquis, M., Averyt, K., Tignor, M., Miller, H. (Eds.), Climate Change 2007: The Physical Science Basis. Contribution of Working Group I to the Fourth Assessment Report of the Intergovernmental Panel on Climate Change. Cambridge University Press, Cambridge, United Kingdom and New York, NY, USA.

Mitrovica, J.X., Peltier, W.R., 1991. On postglacial geoid subsidence over the equatorial oceans. J. Geophys. Res., Solid Earth 96 (B12), 20053–20071.

Munk, W., 2002. Twentieth century sea level: an enigma. Proc. Natl. Acad. Sci. USA 99 (10), 6550–6555.

Nakada, M., Okuno, J., Yokoyama, Y., 2016. Total meltwater volume since the Last Glacial Maximum and viscosity structure of Earth's mantle inferred from relative sea level changes at Barbados and Bonaparte Gulf and GIA-induced J2. Geophys. J. Int. 204 (2), 1237–1253.

Patton, H., Hubbard, A., Andreassen, K., Winsborrow, M., Stroeven, A.P., 2016. The build-up, configuration, and dynamical sensitivity of the Eurasian ice-sheet complex to Late Weichselian climatic and oceanic forcing. Quat. Sci. Rev. 153, 97–121.

Peltier, W., Fairbanks, R.G., 2006. Global glacial ice volume and Last Glacial Maximum duration from an extended Barbados sea level record. Quat. Sci. Rev. 25 (23–24), 3322–3337.

Rohling, E.J., 2007. Progress in paleosalinity: overview and presentation of a new approach. Paleoceanogr. Paleoclimatol. 22 (3).

Rohling, E.J., Bigg, G.R., 1998. Paleosalinity and δ^{18}O: a critical assessment. J. Geophys. Res. 103 (C1), 1307–1318.

Schmidt, G.A., 1999. Error analysis of paleosalinity calculations. Paleoceanography 14 (3), 422–429.

Simms, A.R., Lisiecki, L.E., Gebbie, G., Whitehouse, P., Clark, J.F., 2019. Balancing the Last Glacial Maximum (LGM) sea-level budget. Quat. Sci. Rev. 205, 143–153.

Skinner, L.C., Shackleton, N.J., 2005. An Atlantic lead over Pacific deep-water change across Termination I: implications for the application of the marine isotope stage stratigraphy. Quat. Sci. Rev. 24 (5–6), 571–580.

Smith, W.H., Sandwell, D.T., 1997. Global sea floor topography from satellite altimetry and ship depth soundings. Science 277 (5334), 1956–1962.

Waelbroeck, C., Paul, A., Kucera, M., Rosell-Melé, A., Weinelt, M., Schneider, R., Mix, A., Abelmann, A., Armand, L., Bard, E., et al., 2009. Constraints on the magnitude and patterns of ocean cooling at the Last Glacial Maximum. Nat. Geosci. 2 (2), 127–132.

Wijffels, S., Schmitt, R., Bryden, H., Stigebrandt, A., 1992. Transport of freshwater by the oceans. J. Phys. Oceanogr. 22 (2), 155–162.

Wunsch, C., Stammer, D., 1998. Satellite altimetry, the marine geoid, and the oceanic general circulation. Annu. Rev. Earth Planet. Sci. 26, 219–253.

Yokoyama, Y., Lambeck, K., Deckker, P.D., Johnston, P., Fifield, L., 2000. Timing of the Last Glacial Maximum from observed sea-level minima. Nature 406 (6797), 713–716.